Attribution and mitigation of heat wave-induced urban heat storage change

Attribution and mitigation of heat wave-induced urban heat storage change

Environmental Research Letters

LETTER

Attribution and mitigation of heat wave-induced urban heat storage change

Ting Sun[1,2,6], Simone Kotthaus[1,3], Dan Li[4], H C Ward[1], Zhiqiu Gao[5], Guang-Heng Ni[2] and C S B Grimmond[1,6]

1 Department of Meteorology, University of Reading, Reading, United Kingdom
2 State Key Laboratory of Hydro-Science and Engineering, Department of Hydraulic Engineering, Tsinghua University, Beijing, People's Republic of China
3 Institut Pierre Simon Laplace, Ecole Polytechnique, Palaiseau, France
4 Department of Earth and Environment, Boston University, Boston, United States of America
5 State Key Laboratory of Atmospheric Boundary Layer Physics and Atmospheric Chemistry, Institute of Atmospheric Physics, Chinese Academy of Sciences, Beijing, People's Republic of China
6 Author to whom any correspondence should be addressed.

E-mail: ting.sun@reading.ac.uk and c.s.grimmond@reading.ac.uk

OPEN ACCESS

RECEIVED
5 July 2017

REVISED
14 September 2017

ACCEPTED FOR PUBLICATION
10 October 2017

PUBLISHED
1 November 2017

Keywords: heat wave, heat storage, urban environment, surface energy balance

Abstract

When the urban heat island (UHI) effect coincides with a heat wave (HW), thermal stress in cities is exacerbated. Understanding the surface energy balance (SEB) responses to HWs is critical for improving predictions of the synergies between UHIs and HWs. This study evaluates observed SEB characteristics in four cities (Beijing, Łódź, London and Swindon), along with their ambient meteorological conditions, for both HW and background summer climate scenarios. Using the Analytical Objective Hysteresis Model (AnOHM), particular emphasis is on the heat storage. The results demonstrate that in London and Swindon the amount of daytime heat storage and its fraction relative to the net all-wave radiation increase under HWs. Results further demonstrate that such increases are strongly tied to lower wind speeds. The effects of different UHI mitigation measures on heat storage are assessed using AnOHM. Results reveal that use of reflective materials and maintaining higher soil moisture availability can offset the adverse effects of increased heat storage.

1. Introduction

Heat waves (HWs) are long-lasting, excessively warm periods (Robinson 2001). They are amongst the major causes of weather-related mortality, both regionally and globally (Jones *et al* 2015). Cities are well known to be warmer than their peripheries, commonly referred to as the urban heat island (UHI) effect. Urban features which contribute to the UHI (e.g. low surface water availability, intense anthropogenic activities) may respond to HWs in a nonlinear way that further exacerbates thermal stresses in cities (Li and Bou-Zeid 2013, Zhao *et al* 2014). A recent observational study highlights the role of wind in such interactions, with changes in wind speed leading to enhanced UHIs under HWs in Beijing (Li *et al* 2016).

To understand the enhancement of thermal stresses caused by HWs, we need to examine the surface energy balance (SEB), which, when neglecting horizontal advection and applied to the urban canopy layer, is as follows (Oke 1987):

$$Q^* + Q_F = Q_H + Q_E + \Delta Q_S \quad (1)$$

where Q^* is the net all-wave radiation, defined as $Q^* = K_\downarrow - K_\uparrow + L_\downarrow - L_\uparrow$, with $K_\downarrow$, $K_\uparrow$, $L_\downarrow$ and $L\uparrow$ denoting the incoming shortwave radiation, outgoing shortwave radiation, incoming longwave radiation and outgoing longwave radiation, respectively; the anthropogenic heat flux (Q_F) is the additional energy released by human activities, which can be large in cities (Sailor 2011, Nie *et al* 2014, Chow *et al* 2014); the turbulent sensible heat flux (Q_H) is the major heating source for the atmosphere, while Q_E is the turbulent latent heat flux into the atmosphere due to surface evaporation and/or plant transpiration; ΔQ_S is the net flux of

Table 1. Site characteristics of area around the urban flux towers analysed.

Site	Beijing (China)[a]	Łódź (Poland)	London (UK)	Swindon (UK)
Flux tower location	39.97 °N 116.37 °E	51.77 °N 19.45 °E	51.50 °N 0.12 °W	51.58 °N 1.80 °W
Classification	Urban	Urban	Urban	Suburban
Description	High density business district	High density central business district	High density central business district	Low-rise residential
Source area extent[b]	14 km	5 km	1 km	0.7 km
Surface cover in source area (%)				
Impervious	73	69	81	49
Vegetation	5	31	5	45
Open water	0	0	14	0
Bare soil	22	0	0	6
Study Period	2009–2010	2001–2002	2011–2012	2011–2012
References	Wang *et al* (2014)	Offerle *et al* (2006)	Kotthaus and Grimmond (2012, 2014a, 2014b)	Ward *et al* (2013)

[a] Flux measurements at the Beijing site are available at three levels (i.e. 47 m, 140 m and 280 m), of which measurements at 140 m were used this study (Miao *et al* 2012).

[b] Turbulent flux source area extent (radius) based on climatology weighting of: Łódź: 90%; London and Swindon: 80%; Beijing unspecified.

heat stored within the urban canopy volume, including various urban facets (roofs, walls, ground, etc.).

The responses of SEB to HWs are crucial to understanding the role of urban-atmosphere interactions in governing the synergies between UHIs and HWs (Li *et al* 2015b). Given the much larger magnitude of heat storage in urban areas compared to many other environments (Grimmond and Oke 1999b), Li *et al* (2015b) investigated the response of the storage term to HWs in Beijing. They found that during HWs the heat storage is increased in cities (Li *et al* 2015b). This study, though, is based on observations in a single city (i.e. Beijing). More importantly, mechanisms and controlling factors responsible for such responses remain unknown.

Our study investigates urban SEB characteristics under HWs and background summer climate (June–July–August days excluding HW days, termed as 'BC'). The objective is to identify differences in heat storage between HW and BC conditions using measured SEB characteristics in four cities and to investigate controlling factors including atmospheric conditions and urban characteristics. The impact of different UHI mitigation measures on urban heat storage is then examined.

2. Methodology

2.1. Flux and ambient meteorological measurement

SEB observations from four urban flux towers are used in this study (table 1). The data include measurements of radiative and turbulent heat fluxes, and standard meteorological variables such as air temperature and wind speed. The four sites, located in Beijing (China), Łódź (Poland), London (United Kingdom) and Swindon (United Kingdom), have different surface characteristics (table 1). Observations from all sites have been described extensively elsewhere so details on the instrumentation and setup are not repeated here (table 1). In this study, ΔQ_S is estimated as the residual of the SEB ($Q^*-Q_H-Q_E$). We note that although Q_F can be estimated using models (Allen *et al* 2011, Sailor 2011, Chow *et al* 2014, Nie *et al* 2014), they often carry considerable uncertainty. Hence Q_F is not specifically accounted for in this study. This implies that our results are conservative estimates of ΔQ_S, as Q_F, an additional energy source, is likely to be large especially under HWs (e.g. more air conditioning use) (Stone 2012).

2.2. Heat wave identification

Several definitions of HW are used in the literature (e.g. Robinson 2001, Souch and Grimmond 2004, Perkins 2015). Here, a location-specific definition (Meehl and Tebaldi 2004) is adopted to identify HW periods based on two thresholds of daily maximum air temperature (T_{max}): T_1 the 97.5th percentile, and T_2 the 81st percentile. A HW is defined as the longest period satisfying the following three conditions: (1) $T_{max} > T_1$ for at least 3 days; (2) $\bar{T}_{max} > T_1$ for the entire period; and (3) $T_{max} > T_2$ for the entire period, where $\bar{T}_{max}$ denotes the average of T_{max} over the HW period. This definition is used in many other studies with minor alterations in the selection of T_1 and T_2 (e.g. Lau and Nath (2012, 2014)). To identify HW periods, World Meteorological Organization (WMO) weather stations with long time series of air temperature near the study sites are used (table 2).

2.3. Attribution to ambient forcing variables

HWs are generally characterized by larger solar radiation ($K_\downarrow$), higher air temperature (T_a) and lower wind speed (WS) compared to BC conditions (Meehl and Tebaldi 2004, Miralles *et al* 2014). All three variables are important, given that $K_\downarrow$ directly drives the SEB system, T_a indicates the ambient thermal conditions, and WS implies the advection and convection efficiency.

Table 2. Long term air temperature data of WMO stations used to identify HW events during the study period.

Site	Beijing (China)	Łódź (Poland)	London (UK)	Swindon (UK)
Weather station location	40.07 °N 116.59 °E	51.73 °N 19.40 °E	51.48 °N 0.45 °W	51.76 °N 1.58 °W
Distance to flux tower (km)	21.8	5.1	23.3	24.8
WMO code[a]	54511	12465	03772	03649
Data range (yyyy mm dd)	19730101–20141231	19340329–20141231	19481201–20141231	19510801–20141231
HW duration in study period (days)	48	25	20	25
Number of HW events	5	4	4	4
Date ranges of HW events (yyyy mm dd)	(1) 20090619–20090705 (2) 20090810–20090815 (3) 20100702–20100709 (4) 20100720–20100801 (5) 20100814–20100817	(1) 20010713–20010716 (2) 20010814–20010822 (3) 20020618–20020621 (4) 20020727–20020803	(1) 20110731–20110803 (2) 20110928–20111003 (3) 20120722–20120726 (4) 20120816–20120820	(1) 20110730–20110803 (2) 20110927–20111003 (3) 20120522–20120527 (4) 20120721–20120727

[a] WMO site information refers to: www.wmo.int/pages/prog/www/ois/volume-a/vola-home.htm.

To attribute changes in heat storage from BC to HW to these variables, the Analytical Objective Hysteresis Model (AnOHM, for details refer to Sun *et al* (2017)) is used. AnOHM estimates the storage heat flux (ΔQ_S) from net all-wave radiation (Q^*) following the Objective Hysteresis Model (Grimmond *et al* 1991). One of the major merits of AnOHM is its ability to explicitly account for surface properties in the analytical solution to the heat conduction-advection equation within the SEB framework. This allows attribution of changes in ΔQ_S to different forcing variables (e.g. solar radiation, air temperature, etc.) as well as surface properties (e.g. surface albedo, thermal conductivity, etc.). The applicability of AnOHM over different land cover types has been extensively evaluated (Sun *et al* 2017).

For a specific indicator, X, in the SEB, changes in X (denoted as ΔX) induced by changes in the ambient forcing variables $K_{\downarrow}$, T_a and WS) ambient forcing variables considered (the approximation sign is used here due to the neglect of higher-order terms), can be calculated by AnOHM using:

$$\Delta X \approx \frac{\partial X}{\partial K_{\downarrow}}\Delta K_{\downarrow} + \frac{\partial X}{\partial T_a}\Delta T_a + \frac{\partial X}{\partial WS}\Delta WS. \quad (2)$$

The contributions to ΔX by the different ambient forcing mechanisms, i.e. $\Delta X_{K\downarrow}$, ΔX_{T_a} and ΔX_{WS} related to changes in $K_{\downarrow}$, T_a and WS, respectively, are thus given by

$$\Delta X_{K_{\downarrow}} = \frac{\partial X}{\partial K_{\downarrow}}\Delta K_{\downarrow}, \quad (3)$$

$$\Delta X_{T_a} = \frac{\partial X}{\partial T_a}\Delta T_a, \quad (4)$$

$$\Delta X_{WS} = \frac{\partial X}{\partial WS}\Delta WS. \quad (5)$$

3. Contrasting urban SEB responses to HWs in four cities

To analyze differences in SEB between BC and HW conditions, the radiative and turbulent fluxes are separately averaged for HW and BC days and the differences between HW and BC conditions (i.e. HW–BC) are compared at each site (figure 1). The median and interquartile range (IQR) of turbulent fluxes differ among the four sites: sensible heat fluxes are observed to increase in Beijing, Łódź and Swindon, and decrease in London under HWs (figure 1(*a*)); while latent heat fluxes are found to increase in Beijing, and remain unchanged in London, Swindon and Łódź (figure 1(*b*)). Although the responses of turbulent fluxes vary from site to site, daytime increases in heat storage (figure 1(*c*)) and net all-wave radiation (figure 1(*d*)) are observed at all four sites, though the increase in the former is small in Łódź.

Two indicators are used to further examine the energy partitioning: the evaporative fraction EF ($= Q_E/(Q_H + Q_E)$) and the heat storage ratio rQ_S ($= \Delta Q_S/Q^*$). The focus is the midday period (10:00–14:00 local standard time, hour ending data) when the surface fluxes are the largest and EF and rQ_S are numerically stable. The EF values are largely unchanged (figure 2(*a*)) at the four study sites, suggesting a small impact of HWs on the partitioning of the turbulent fluxes: the changes remain proportionally similar between the sensible and latent fluxes. However, rQ_S experiences distinct changes between HW and BC conditions across the four sites: the median differences vary from minimal (< 0.05 at Beijing and Łódź) to considerable increases ($\sim$0.25 at London; $\sim$0.15 at Swindon) (figure 2(*b*)). Considering the increase in Q^* during HWs (figure 1(*d*)), an unchanged rQ_S implies a proportional increase in heat storage. Higher rQ_S, however, implies a further increase in heat storage: not

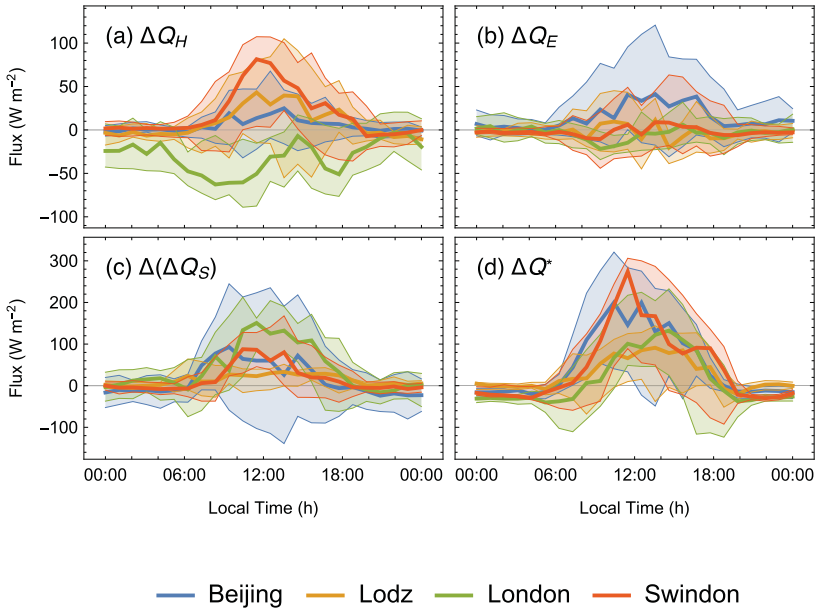

Figure 1. Interquartile range (shaded) and median (lines) differences (Δ) between heat wave (HW) and background summer climate (BC) conditions in terms of: (*a*) turbulent sensible heat flux Q_H, (*b*) turbulent latent heat flux Q_E, (*c*) net heat storage ΔQ_S, and (*d*) net all-wave radiation Q^* at the four study sites (table 1).

only is more energy supplied, but also a larger portion of the input energy is stored during the daytime. This may cause increased heat release to the atmosphere at night and/or in the post-HW periods, thereby causing higher thermal stresses at night and/or extending the duration of hot conditions in cities (Li and Bou-Zeid 2013).

4. Changes in ambient meteorological conditions

Figure 3 shows the differences in the ambient meteorological conditions between HW and BC conditions. As expected, increases in the incoming solar radiation $K_{\downarrow}$ (figure 3(*a*)) and air temperature T_a are observed under HWs (figure 3(*c*)), which are usually associated with anti-cyclonic conditions (Meehl and Tebaldi 2004). In agreement with the small heat-storage increment observed at Łódź (figure 1(*c*)), the diurnal amplitude of temperature difference is very small. Meanwhile, small changes in the incoming longwave radiation $L_{\downarrow}$ are observed (figure 3(*b*)). In Łódź, the specific humidity q_a is considerably higher under HW than BC conditions, unlike the other sites where the difference is small. Given the importance of humidity to emissivity (e.g. Jonsson *et al* 2006) the more humid condition may lead to the higher $L_{\downarrow}$ at Łódź under HW conditions.

Changes in wind speed *WS* from BC to HW (figure 3(*d*)) differ among the four sites: *WS* decreases at London and Swindon, but increases at Beijing and shows little change at Łódź. This can be explained by the site locations relative to the meso-scale weather patterns over Europe and China, respectively, based on the ERA-Interim dataset (Dee *et al* 2011). The center of the anticyclone is found near the European study sites during their respective HW periods. While this has a calming effect on the winds observed over the British Isles where strong marine winds are common, no clear impact is detected on the central European site (i.e. Łódź) where wind speeds are generally lower (not shown). High pressure systems consistently form over Eastern China during HW periods, so that stronger winds are induced over Beijing with potential influence of the nearby sea. The large-scale flow in combination with the local valley-breeze system around this Asian megacity appears to restrict the heat-storage ratio during HWs to be at the same level found during BC. Note that only the sites where wind speeds are reduced during the HW, i.e. London and Swindon, show a clearly increased heat storage ratio (figure 2(*b*)), suggesting that the reduction in wind speed, which is observed in London and Swindon but not in Beijing (where *WS* was increased) or Łódź (where *WS* was already low), controls the increase in heat storage ratio.

5. Impact of atmospheric forcing on the heat storage ratio

5.1. Attribution analysis

To examine the impact of atmospheric forcing on rQ_S, rQ_S is first simulated by AnOHM at the four sites (figure 4) using the average meteorological conditions as inputs. Again, HW and BC conditions are separated. At all sites, lower *WS* consistently leads to an increase in rQ_S and vice versa. Further, it is evident that rQ_S responds differently to the transition from BC to

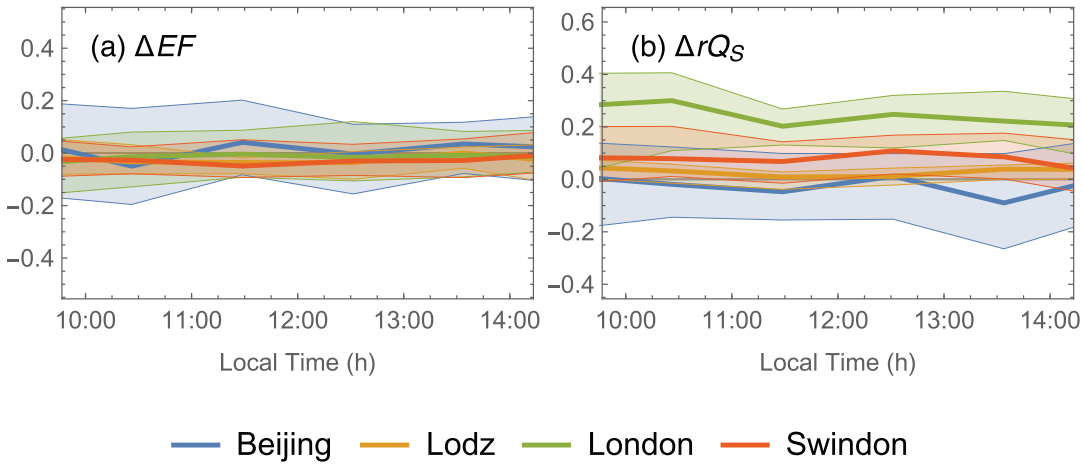

Figure 2. Differences (Δ) in (*a*) evaporative fraction $EF = Q_E/(Q_H + Q_E)$ and (*b*) heat storage ratio ($rQ_S = \Delta Q_S/Q^*$) between HW and BC conditions at the four study sites (table 1). See figure 1 for other details.

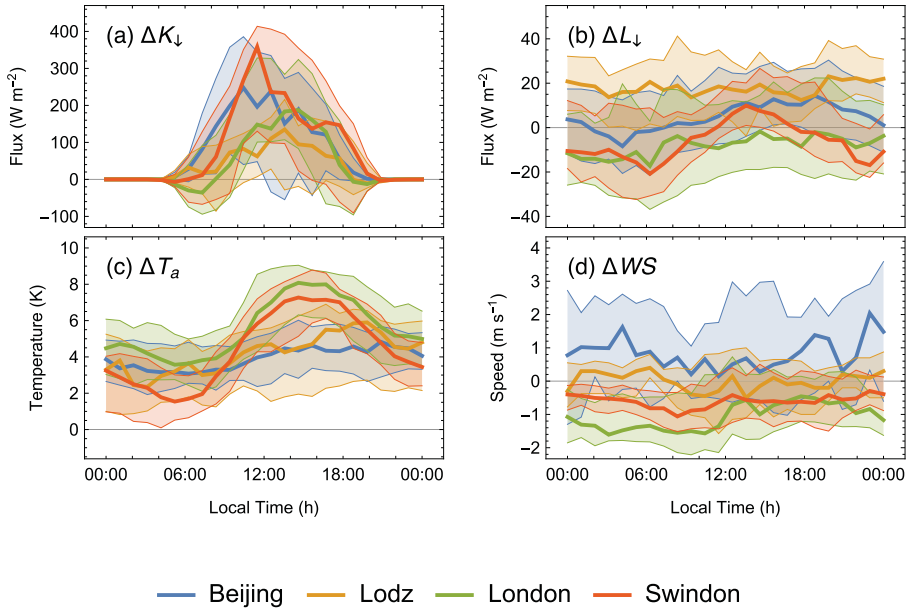

Figure 3. Differences in the ambient meteorological conditions between HW and BC conditions: (*a*) incoming solar radiation $K_{\downarrow}$, (*b*) incoming longwave radiation $L_{\downarrow}$, (*c*) air temperature T_a, and (*d*) wind speed *WS* at the four study sites (table 1). See figure 1 for other details.

HW across the four sites. This is probably caused by a combination of the impact of surface characteristics (see Appendix) and other atmospheric forcing variables.

The changes of rQ_S from BC to HW simulated by AnOHM are decomposed to quantify contributions from three key ambient meteorological forcing variables (i.e. $K_{\downarrow}$, T_a and *WS*), (see section 2.3), and compared to the observed changes at the four study sites (figure 5). It is evident that $K_{\downarrow}$ and T_a contribute to the changes in rQ_S in an opposite way at all sites: an increased $K_{\downarrow}$ lowers rQ_S whereas a higher T_a increases rQ_S. Furthermore, except for Łódź where the changes in *WS* between BC and HW conditions are minimal, *WS* consistently forms the largest contribution to the changes in rQ_S at the other three sites (i.e. Beijing, London and Swindon). Again, it is found a lower *WS* leads to an increased rQ_S (as in London and Swindon) and vice versa (as in Beijing).

This attribution analysis implies that the stagnant conditions associated with HWs (e.g. in Europe, Tressol *et al* (2008) have the potential to induce an increased heat storage ratio in urban areas. Furthermore, given urban wind reductions (Oke 1987, Grimmond and Oke 1999a, Britter and Hanna 2003, Vautard *et al* 2010, Liu *et al* 2017), cities are more likely to experience an increased heat storage ratio. However, for places where wind speeds are enhanced during HWs, the heat storage ratio might be reduced compared to BC conditions.

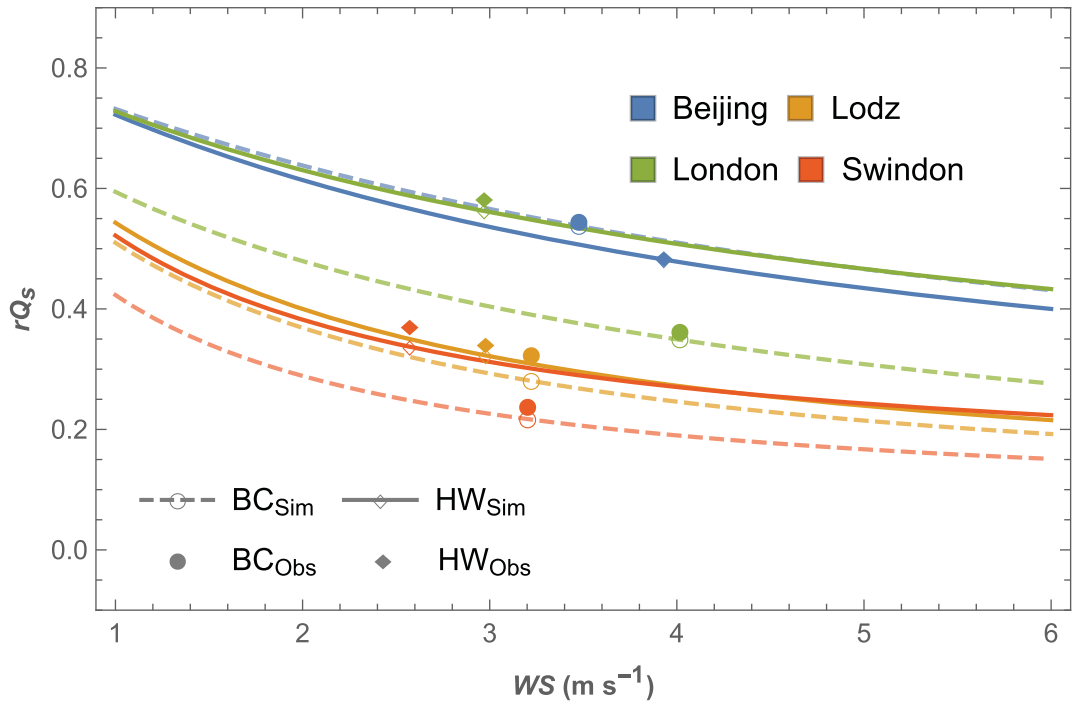

Figure 4. Midday (10:00-14:00 h) heat storage ratio $rQ_S = \Delta Q_S/Q^*$ derived by AnOHM for BC (dashed lines) and HW conditions (solid lines) for the four study sites (table 1) as a function of wind speed *WS*. Symbols mark rQ_S at average observed wind speed at the different sites with empty (filled) circles and diamonds representing the simulated (observed) states under BC and HW, respectively.

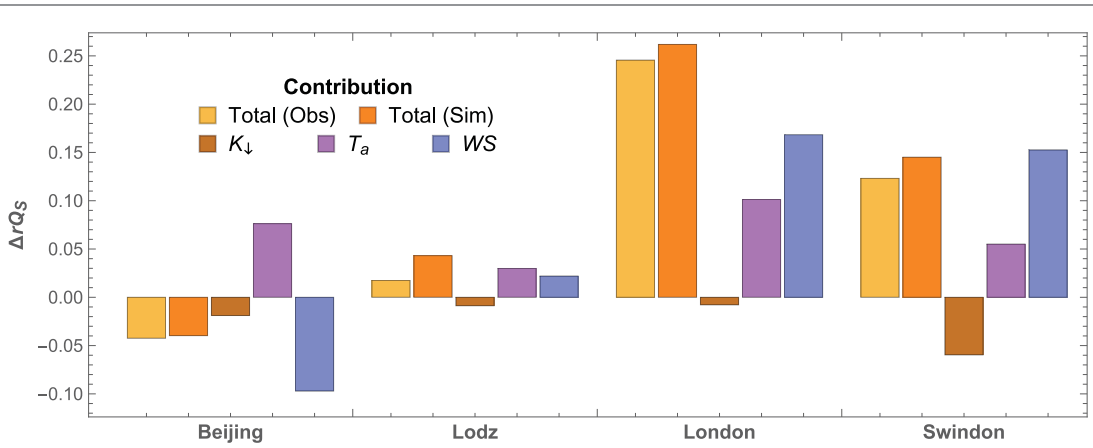

Figure 5. Attribution of changes in rQ_S between BC and HW conditions for the four study sites (table 1). For comparison, the observed changes in rQ_S are also shown.

5.2. Effects of mitigation measures

To address enhanced thermal stresses in cities, different mitigation measures have been implemented, of which reflective building materials (e.g. white roofs, reflective walls, etc.) and green infrastructure (e.g. trees, green roofs, etc.) are widely used and found to be effective under some conditions (Saadatian *et al* 2013, Georgescu *et al* 2014, Yang *et al* 2015, Sun *et al* 2016). Here, changes in rQ_S from BC to HW for two mitigation scenarios that involve alterations of surface characteristics are examined: albedo α (reflective material scenario, red dashed lines in figure 6) and Bowen ratio β (vegetation cover scenario, blue solid lines in figure 6). Note that for the vegetation cover scenario, the effects of surface roughness change are excluded in order to focus on the role of surface wetness in moderating rQ_S. The impacts of surface roughness (including vegetation) on wind profiles can be found in Kent *et al* (2017b).

For the reflective material scenario, a higher albedo can result in a higher rQ_S, implying that a larger portion of energy would be stored in urban surfaces. However, we find ΔQ_S in fact decreases since Q^* is decreased with increasing α (not shown) and the decrease in Q^* is disproportionately larger than the decrease in ΔQ_S: this decrease in Q^* is directly caused by the reduced net shortwave radiation (i.e. $(1-\alpha)K_{\downarrow}$) as α increases, whereas the decrease in ΔQ_S is induced by the smaller

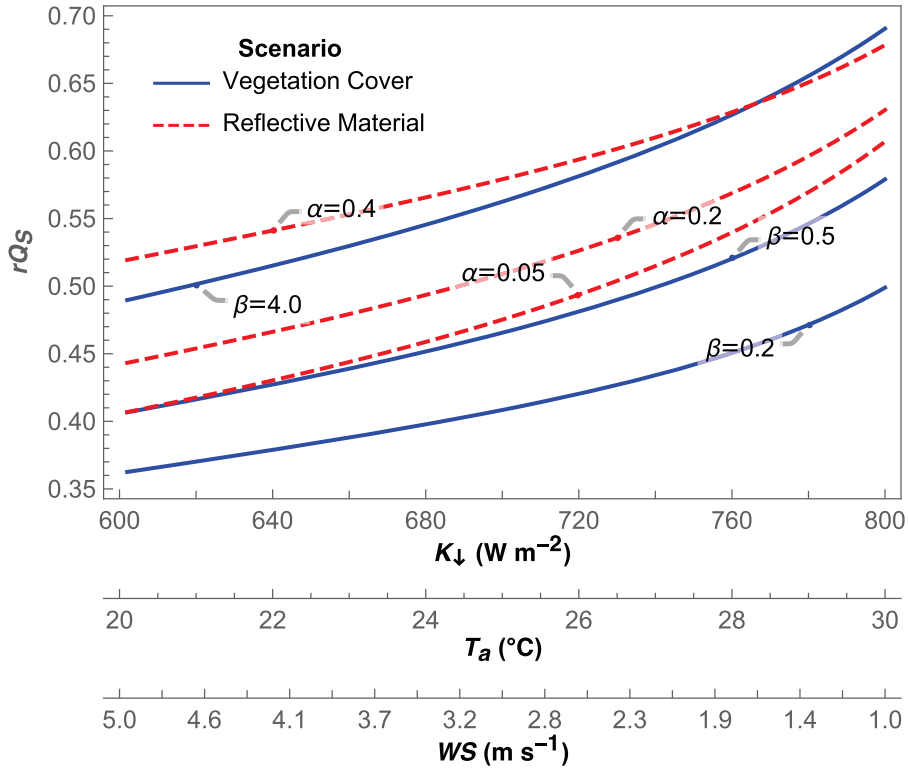

Figure 6. AnOHM-simulated variations in rQ_S under typical BC (left side) to HW (right side) conditions for different mitigation scenarios: reflective material (represented by surface albedo α) and vegetation cover (represented by Bowen ratio β).

temperature gradient due to the lower surface temperature T_s.

For the vegetation cover scenario, a lower β indicates more turbulent energy will be dissipated as latent heat rather than sensible heat, directly leading to a decrease in the surface temperature T_s. As such, for a given surface whose internal temperature responds more slowly to the forcing, the decrease in the temperature gradient caused by a lower surface temperature can result in a decrease in ΔQ_S. However, the change in Q^* caused by surface temperature is minimal due to the secondary role of outgoing longwave radiation $L\uparrow$ ($= \varepsilon\sigma T_s^4$, ε is the surface emissivity, σ is Stefan–Boltzmann constant) in Q^*. The reduction in β thus results in a lower rQ_S.

Thus, although rQ_S might increase under HWs, it can be modulated by different mitigation measures. Using reflective materials can help reduce energy input and subsequently the heat storage despite an increase in rQ_S. Increasing vegetative infrastructure redistributes more energy to latent heat and thus leads to a lower heat storage ratio rQ_S. Since a higher rQ_S implies more energy is stored in cities (under constant Q^*), increased vegetation may help remove heat from the urban area rather than prolonging conditions with increased heat stress.

It should be pointed out that our focus here is on the bulk effect of these mitigation strategies. For example, the analysis did not examine mitigation strategies applied on different urban facets separately. In practice, the effectiveness of mitigation measures depends on a wide range of factors such as urban morphology (Lindberg and Grimmond 2011, Kent *et al* 2017a), hydrometeorological forcing (Sun *et al* 2013), material properties (Kotthaus *et al* 2014, Yang and Wang 2014), and layout configuration (Sun *et al* 2014). To investigate these important issues will require other tools and is left for future work.

6. Concluding remarks

A key finding of this study is that the amount of daytime heat storage as well as its fraction in the net all-wave radiation (i.e. heat storage ratio rQ_S) increases under HWs for cities that experience lower wind speeds, or wind reduction, under HWs. In areas where wind speeds are already low or even enhanced during HWs, the heat storage ratio is not affected or even decreased.

The positive daytime heat storage flux is of particular concern as the accumulated energy is eventually released into the atmosphere at night, leading to an enhanced UHI. Given that the highest mortality risks under HWs are commonly linked to nocturnal conditions (Trigo 2005), this has critical health implications. In addition, heat stored in the urban areas during HWs may be released in the post-HW periods thereby extending the hot conditions in cities (Li and Bou-Zeid 2013).

The techniques and approaches used in this study identify the wind reduction as the predominant contributor to the increase in rQ_S during a typical BC-HW

Table A1. Calibrated parameters of study sites for AnOHM.

Site	Beijing (China)	Łódź (Poland)	London (UK)	Swindon (UK)
Surface albedo α	0.15	0.14	0.15	0.13
Surface emissivity	0.92	0.95	0.92	0.91
Canopy heat capacity C_g (10^6 J m^{-3} K^{-1})	2.4	2.4	2.4	1.8
Canopy thermal conductivity k (W m^{-1} K^{-1})	2.9	1.7	2.8	1.2
Bulk transfer coefficient C_H (W m^{-2} K^{-1})	4.1	5.6	4.2	5.1

transition. Given the observed wind reduction in cities (Liu *et al* 2017) and stagnant conditions associated with HWs (Trigo 2005), the present analysis recognizes the crucial role of wind speed in moderating the urban thermal environment under HWs. Further, the importance of surface water availability in cities during HWs is highlighted as wetter surfaces help to offset adverse effects of increased rQ_S. Appropriate building design to enhance urban wind flow or ventilation (Li *et al* 2015a) could be another effective mitigation method.

Future work should investigate heat storage processes during HWs across a wider range of regional climates and urban characteristics. Long-term flux observations in more cities are critical to expanding our understanding of HWs in urban environments.

Appendix: Calibration of AnOHM

The input data for AnOHM includes diurnal cycles of: (1) incoming solar radiation $K_{\downarrow}$; (2) air temperature T_a; and daily mean: (3) wind speed WS and (4) Bowen ratio β. By setting net all-wave radiation Q^* as the benchmark for model performance, the required parameters for AnOHM can be obtained via calibration, including (1) surface albedo α, (2) surface emissivity, (3) soil/canopy heat capacity C_g, (4) soil/canopy thermal conductivity k, (5) bulk transfer coefficient C_H. To obtain these parameters for study sites (table 1), the characteristics of study sites were assumed not to change over time and data for clear days were used in the calibration. The parameter calibration ranges were limited to literature values (Wang *et al* 2011, Yang *et al* 2014) to avoid unreasonable values. The calibrated results are provided in table A1.

Acknowledgment

SG acknowledges the support from Newton Fund CSSP-China program, EUf7 emBRACE (FP7-ENV-2011 283201), NERC TRUC (NE/L008971/1), NERC ClearfLo (NE/H003231/1) and H2020 Urban Fluxes. TS acknowledges National Science Foundation of China (51679119 and 91647107), China Postdoctoral Science Foundation (2015T80093) and NERC Independent Research Fellowship (NE/P018637/1).

ORCID iDS

Ting Sun https://orcid.org/0000-0002-2486-6146
Simone Kotthaus https://orcid.org/0000-0002-4051-0705
Helen Ward https://orcid.org/0000-0001-8881-185X
Sue Grimmond https://orcid.org/0000-0002-3166-9415
Dan Li https://orcid.org/0000-0001-5978-5381

References

Allen L, Lindberg F and Grimmond C S B 2011 Global to city scale urban anthropogenic heat flux: model and variability *Int. J. Climatol.* **31** 1990–2005
Britter R E and Hanna S R 2003 Flow and dispersion in urban areas *Annu. Rev. Fluid Mech.* **35** 469–96
Chow W T L, Salamanca F P, Georgescu M, Mahalov A, Milne J M and Ruddell B L 2014 A multi-method and multi-scale approach for estimating city-wide anthropogenic heat fluxes *Atmos. Environ.* **99** 64–76
Dee D P *et al* 2011 The ERA-Interim reanalysis: configuration and performance of the data assimilation system *Q.J.R. Meteorol. Soc.* **137** 553–97
Georgescu M, Morefield P E, Bierwagen B G and Weaver C P 2014 Urban adaptation can roll back warming of emerging megapolitan regions *Proc. Natl Acad. Sci. USA* **111** 2909–14
Grimmond C S B and Oke T R 1999a Aerodynamic properties of urban areas derived, from analysis of surface form *J. Appl. Meteorol.* **38** 1262–92
Grimmond C S B and Oke T R 1999b Heat storage in urban areas: local-scale observations and evaluation of a simple model *J. Appl. Meteorol.* **38** 922–40
Grimmond C S B, Cleugh H A and Oke T R 1991 An objective urban heat storage model and its comparison with other schemes *Atmos. Environ. B-Urb.* **25** 311–26
Jones B, O'Neill B C, McDaniel L, McGinnis S, Mearns L O and Tebaldi C 2015 Future population exposure to US heat extremes *Nat. Clim. Change* **5** 652–5
Jonsson P, Eliasson I, Holmer B and Grimmond C S B 2006 Longwave incoming radiation in the tropics: results from field work in three African cities *Theor. Appl. Climatol.* **85** 185–201
Kent C W, Grimmond C S B and Gatey D 2017a Aerodynamic roughness parameters in cities: inclusion of vegetation *J. Wind Eng. Ind. Aerod.* **169** 168–76
Kent C W, Grimmond C S B, Barlow J, Gatey D, Kotthaus S, Lindberg F and Halios C H 2017b Evaluation of urban local-scale aerodynamic parameters: implications for the vertical profile of wind speed and for source areas *Bound.-Layer Meteorol.* **164** 183–213
Kotthaus S and Grimmond C S B 2014a Energy exchange in a dense urban environment—Part I: temporal variability of long-term observations in central London *Urban Clim.* **10** 261–80
Kotthaus S and Grimmond C S B 2014b Energy exchange in a dense urban environment—Part II: impact of spatial heterogeneity of the surface *Urban Clim.* **10** 281–307
Kotthaus S and Grimmond C S B 2012 Identification of micro-scale anthropogenic CO_2, heat and moisture sources—processing eddy covariance fluxes for a dense urban environment *Atmos. Environ.* **57** 301–16
Kotthaus S, Smith T E L, Wooster M J and Grimmond C S B 2014 Derivation of an urban materials spectral library through emittance and reflectance spectroscopy *ISPRS J. Photogramm. Remote Sens.* **94** 194–212

Lau N-C and Nath M J 2012 A model study of heat waves over North America: meteorological aspects and projections for the twenty-first century *J. Clim.* **25** 4761–84
Lau N-C and Nath M J 2014 Model simulation and projection of european heat waves in present-day and future climates *J. Clim.* **27** 3713–30
Li B, Luo Z, Sandberg M and Liu J 2015a Revisiting the 'venturi effect' in passage ventilation between two non-parallel buildings *Build. Environ.* **94** 714–22
Li D and Bou-Zeid E 2013 Synergistic interactions between urban heat Islands and heat waves: the impact in cities is larger than the sum of its parts *J. Appl. Meteorol. Clim.* **52** 2051–64
Li D, Sun T, Liu M, Wang L and Gao Z 2016 Changes in wind speed under heat waves enhance urban heat Islands in the Beijing metropolitan area *J. Appl. Meteorol. Clim.* **55** 2369–75
Li D, Sun T, Liu M, Yang L, Wang L and Gao Z 2015b Contrasting responses of urban and rural surface energy budgets to heat waves explain synergies between urban heat islands and heat waves *Environ. Res. Lett.* **10** 054009
Lindberg F and Grimmond C S B 2011 The influence of vegetation and building morphology on shadow patterns and mean radiant temperatures in urban areas: model development and evaluation *Theor. Appl. Climatol.* **105** 311–23
Liu J, Gao Z, Wang L, Li Y and Gao C Y 2017 The impact of urbanization on wind speed and surface aerodynamic characteristics in Beijing during 1991–2011 *Meteorol. Atmos. Phys.* **10** 1–14
Meehl G A and Tebaldi C 2004 More intense, more frequent, and longer lasting heat waves in the 21st century *Science* **305** 994–7
Miao S, Dou J, Chen F, Li J and Li A 2012 Analysis of observations on the urban surface energy balance in Beijing *Sci. China Earth Sci.* **55** 1881–90
Miralles D G, Teuling A J, van Heerwaarden C C and de Arellano J V-G 2014 Mega-heatwave temperatures due to combined soil desiccation and atmospheric heat accumulation *Nat. Geosci.* **7** 345–9
Nie W-S, Sun T and Ni G-H 2014 Spatiotemporal characteristics of anthropogenic heat in an urban environment: a case study of tsinghua campus *Build. Environ.* **82** 675–86
Offerle B D, Grimmond C S B, Fortuniak K, Klysik K and Oke T R 2006 Temporal variations in heat fluxes over a central European city centre *Theor. Appl. Climatol.* **84** 103–15
Oke T R 1987 *Boundary Layer Climates* (Abingdon: Taylor and Francis)
Perkins S E 2015 A review on the scientific understanding of heatwaves—Their measurement, driving mechanisms, and changes at the global scale *Atmos. Res.* **164–165** 242–67
Robinson P J 2001 On the definition of a heat wave *J. Appl. Meteorol.* **40** 762–75
Saadatian O, Sopian K, Salleh E, Lim C H, Riffat S, Saadatian E, Toudeshki A and Sulaiman M Y 2013 A review of energy aspects of green roofs *Renew. Sustain. Energy Rev.* **23** 155–68
Sailor D J 2011 A review of methods for estimating anthropogenic heat and moisture emissions in the urban environment *Int. J. Climatol.* **31** 189–99
Souch C and Grimmond C S B 2004 Applied climatology: heat waves *Prog. Phys. Geog.* **28** 599–606
Stone B Jr 2012 *The City and the Coming Climate* (Cambridge: Cambridge University Press)
Sun T, Bou-Zeid E and Ni G-H 2014 To irrigate or not to irrigate: Analysis of green roof performance via a vertically-resolved hygrothermal model *Build. Environ.* **73** 127–37
Sun T, Bou-Zeid E, Wang Z-H, Zerba E and Ni G-H 2013 Hydrometeorological determinants of green roof performance via a vertically-resolved model for heat and water transport *Build. Environ.* **60** 211–24
Sun T, Grimmond C S B and Ni G-H 2016 How do green roofs mitigate urban thermal stress under heat waves? *J. Geophys. Res-Atmos.* **121** 5320–35
Sun T, Wang Z-H, Oechel W C and Grimmond C S B 2017 The Analytical Objective Hysteresis Model (AnOHM v1.0): methodology to determine bulk storage heat flux coefficients *Geosci. Model Dev.* **10** 2875–90
Tressol M *et al* 2008 Air pollution during the 2003 European heat wave as seen by MOZAIC airliners *Atmos. Chem. Phys.* **8** 2133–50
Trigo R M 2005 How exceptional was the early august 2003 heatwave in France? *Geophys. Res. Lett.* **32** L10701
Vautard R, Cattiaux J, Yiou P, Thépaut J-N and Ciais P 2010 Northern Hemisphere atmospheric stilling partly attributed to an increase in surface roughness *Nat. Geosci.* **3** 756–61
Wang L, Li D, Gao Z, Sun T, Guo X and Bou-Zeid E 2014 Turbulent transport of momentum and scalars above an urban canopy *Bound.-Layer Meteorol.* **150** 485–511
Wang Z-H, Bou-Zeid E, Au S K and Smith J A 2011 Analyzing the sensitivity of WRF's single-layer urban canopy model to parameter uncertainty using advanced monte carlo simulation *J. Appl. Meteorol. Clim.* **50** 1795–814
Ward H C, Evans J G and Grimmond C S B 2013 Multi-season eddy covariance observations of energy, water and carbon fluxes over a suburban area in Swindon, UK *Atmos. Chem. Phys.* **13** 4645–66
Yang J and Wang Z-H 2014 Physical parameterization and sensitivity of urban hydrological models: application to green roof systems *Build. Environ.* **75** 250–63
Yang J, Wang Z-H and Kaloush K E 2015 Environmental impacts of reflective materials_ Is high albedo a silver bullet for mitigating urban heat island? *Renew. Sustain. Energy Rev.* **47** 830–43
Yang J, Wang Z-H, Chen F, Miao S, Tewari M, Voogt J A and Myint S 2014 Enhancing hydrologic modelling in the coupled weather research and forecasting–urban modelling system *Bound.-Layer Meteorol.* **155** 1–23
Zhao L, Lee X, Smith R B and Oleson K 2014 Strong contributions of local background climate to urban heat islands *Nature* **511** 216–9